Analysis of Sampling Errors for Climate Monitoring Satellites

DANIEL B. KIRK-DAVIDOFF

Department of Meteorology, University of Maryland, College Park, College Park, Maryland

RICHARD M. GOODY AND JAMES G. ANDERSON

Division of Engineering and Applied Science, Harvard University, Cambridge, Massachusetts

(Manuscript received 14 October 2003, in final form 1 June 2004)

ABSTRACT

Sampling retrievals of high-accuracy first-moment statistics constitute a central concern for climate research. Considered here is the important case of brightness temperature retrievals from a selection of possible orbits. Three-hourly global satellite brightness temperature data are used to predict the sampling error of monthly to annual mean brightness temperature retrieved by one or more satellites in low earth orbits. A true polar orbit is found to offer substantial advantages over a sun-synchronous orbit in the retrieval of annual mean brightness temperature, since the rotation of the local time of observation through two full diurnal cycles greatly reduces the error due to imperfect sampling of diurnal variations. Thus, a single polar orbiting satellite can produce annual mean, zonal mean brightness temperatures with typical sampling errors of less than 0.1 K, while even three sun-synchronous orbiters have high-latitude errors of up to 0.4 K. The error in retrievals of the annual mean diurnal cycle of brightness temperature is also discussed. In this case, high accuracy ($<$0.1 K) requires three cross-track scanning satellites in precessing orbits, or else a very large number ($\sim$10) of nadir-viewing satellites in precessing orbits. The large sampling errors of sun-synchronous satellites are highly correlated from year to year, so that if equator-crossing times are held fixed, sampling errors in year-to-year differences of annual means are similar for sun-synchronous and precessing orbits.

1. Introduction

Satellite climate observations offer broad and consistent spatial sampling, complementing surface-based observations, which may be compromised by correlations with anthropogenic or natural changes in surface conditions near observation sites, and which may be spatially biased by ease or difficulty of access to a given location on the surface. However, imperfect temporal sampling introduces random errors (due to aperiodic weather noise) and biases that can substantially reduce the accuracy of satellite observations of the state of the atmosphere. Selection of the number of satellites, their orbital configuration, and their scanning pattern all contribute to satellite sampling errors for climate studies. These errors have been carefully investigated for existing climate records (Salby and Callaghan 1997; Christy et al. 2003; Mears et al. 2003; Vinnikov and Grody 2003; Vinnikov et al. 2004). The latter three papers included specific measures to estimate and remove biases contributed by inadequately sampled diurnal variability, either by estimating the strength of various harmonics of the diurnal cycle directly from observations, or by simulating the diurnal cycle using a general circulation model (Mears et al. 2003).

The continuing controversy over the tropospheric temperature record as measured by radiosondes and by the Microwave Sounding Unit (MSU)/Advanced Microwave Sounding Unit (AMSU) instruments illustrates the need for climate observing strategies that can produce absolutely accurate climate data records. Our purpose is to reduce the need for after-the-fact error correction by finding orbits that minimize sampling errors. For interannual trends, much of the bias treated by these authors derives from the drift in the equator-crossing time of sun-synchronous satellites. A theoretical study of sampling errors due to satellite orbital drift for a constellation of three sun-synchronous orbits was made by Leroy (2001), for the case of clear skies and large-amplitude diurnal variability in surface temperature. He showed that asymmetry in the time of observations for ascending and descending orbit legs caused substantial errors in high latitude regions even for three equally spaced satellites, due to aliasing of the semidiurnal cycle onto the long-term mean. He also showed

Corresponding author address: Dr. Daniel Kirk-Davidoff, Department of Meteorology, University of Maryland, College Park, 3423 Computer and Space Sciences Building, College Park, MD 20742. E-mail: dankd@atmos.umd.edu

that that cross-track scanning of practical width did little to reduce this sampling bias. We extend this work using a more realistic proxy dataset, and consider both bias and short term climate variability in order to determine which constellation of satellites in which orbital configuration are capable of adequately sampling radiance observations so as to obtain accurate climate means. The climate means investigated include annual and seasonal mean brightness temperature, as well as annual mean diurnal brightness temperature maximum, minimum, and range.

2. Methods

We consider the retrieval of brightness temperature by a highly accurate nadir-viewing satellite with a footprint of 50 km. In some cases, a cross-track scanning instrument is simulated by assuming that a detector array allows multiple measurements to the left and right of the nadir (25 observations, spaced by 1° in longitude, centered on the nadir point). Our method is to calculate the location of the suborbital point over the course of one year, and to use archived satellite brightness temperatures to determine the brightness temperature retrieved by our simulated orbiter at each time. This establishes the "observed" brightness temperatures, which are then grouped by location, and averaged together over periods from a month to a year. All archived brightness temperatures are then grouped by location and averaged together over the same time periods, establishing the "true" brightness temperature. The difference between the observed and true brightness temperatures establishes the accuracy of the retrieval.

For our archive, we use the Salby Global Cloud Imagery (GCI) dataset (Salby et al. 1991), a regridded compilation of 11-μm brightness temperatures retrieved from geostationary and polar orbiting satellites. It has a spatial resolution of 0.35° latitude and 0.70° longitude, or 512 $\times$ 512 grid points, and a temporal resolution of 3 h. The 11-μm region has the advantage, for our purposes, of being one of the most highly variable regions in the terrestrial spectrum, thus providing a worst-case example for retrieval of long-term climate statistics. Being minimally affected by water vapor or carbon dioxide, this band essentially measures the temperature of the highest cloud layer, or of the surface, in the absence of clouds. Other bands, which mostly represent emission by water vapor or carbon dioxide high in the atmosphere, have variances several times smaller (Haskins et al. 1999). Thus, a satellite or set of satellites that can accurately retrieve 11-μm brightness temperature can certainly retrieve other bands to higher accuracy, all other errors being equal.

A satellite orbiting about the earth remains in a plane whose orientation is fixed with respect to the stars, except to the extent that this orbital plane is perturbed by such things as atmospheric drag, radiation pressure of sunlight, and the earth's departures from perfect sphericity. We consider only the perturbation due to the first zonal harmonic perturbation to the earth's shape, J_2. Assuming a circular orbit, this perturbation will affect only the angular orientation of the satellite's plane of orbit with respect to the stars (Heiskanen and Moritz 1967):

$$\Omega' = \frac{3na_e^2 J_2}{2a^2}\cos i, \tag{1}$$

where Ω' is the rate of change of the angular orientation of the satellite's plane of orbit in rad s^{-1}, $J_2 = 1.08 \times 10^{-3}$, $n = \sqrt{GM/a^3}$ is the orbital velocity in rad s^{-1}, a_e is the earth's radius, a is the radius of the satellite's orbit, G is the gravitational constant, M is the mass of the earth, and i is the inclination of the satellite's orbit with respect to the equator. We assume an aperture of 0.060 rad, which for an orbit altitude of 833 km, yields a footprint about 50 km wide, similar to the resolution of the Salby dataset and some satellites (e.g., IRIS; Hanel et al. 1972). Assuming a 10-s averaging period yields (again, for an 833-km orbit) a length of 74 km, or about two grid squares.

Once the satellite's orbital plane and its initial position is known, we can locate the region at the surface sampled at any instant:

$$\phi = \arcsin(\sin\phi_1 \cos d + \cos\phi_1 \sin d) \tag{2}$$

$$\lambda = \lambda_1 - \arctan\left(\frac{\sin d \cos\phi_1}{\cos d - \sin\phi \sin\phi_1}\right) + t(\Omega - \Omega'), \tag{3}$$

where ϕ is the latitude, ϕ_I is the initial latitude, d is the distance along the orbit in radians, λ is the longitude, λ_I is the initial longitude, t is the time elapsed since the initial position, and Ω is the earth's angular rotation rate equal to 7.292 x10^{-5} rad s^{-1}.The initial motion is assumed to be purely eastward (so that the initial latitude is also the orbital inclination and the poleward limit of motion), unless the satellite is in a polar orbit, in which case the motion is southward. Radiances at a given location and time are linearly interpolated from the nearest neighbor time steps. When satellite-sampled averages and complete averages are to be binned by local time before comparison (as for comparison of the amplitude of the diurnal variability), the proxy data are also interpolated to higher temporal resolution before being assigned to a local time bin for averaging.

Sampling of the diurnal cycle differs for polar orbits, sun-synchronous orbits (e.g., IRIS, with an inclination of 99°; Hanel et al. 1972) and low-inclination precessing orbits (e.g., TRMM, with an inclination of 35°; Chang et al. 1998), as illustrated in Fig. 1. A polar-orbiting satellite remains in a fixed orbital plane, sampling points at each latitude at two local times, approximately 12

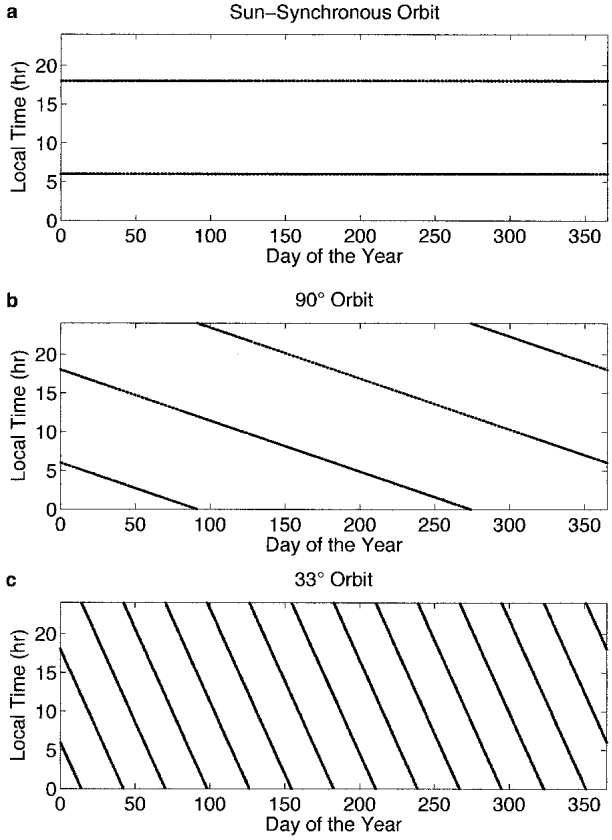

FIG. 1. Equator-crossing times as a function of Julian date for three different orbits, as indicated.

h apart. These local times cycle through 24 hours in the course of a year, as the plane of the satellites orbit rotates with respect to the earth–sun line. A sun-synchronous satellite orbits in a plane fixed with respect to the earth–sun line, and so samples at two discrete, fixed times throughout the year. A low-latitude orbiter's orbital plane rotates relatively rapidly with respect to the sun–earth line, and so such a satellite can sample the entire diurnal cycle several times each year (six for an inclination of 33° and an altitude of 662 km).

3. Dataset characteristics

The 11-μm brightness temperature is essentially a measure of cloud-top temperature, or of sea- or land-surface temperature for clear air. As shown in Fig. 2a, brightness temperature is at a minimum over Antarctica, at a local minimum near the equator, where deep convection is strongest, and at a maximum over the subtropical deserts. Variability (shown in Fig. 2b) is strongest in the equatorial belt, where hourly brightness temperature values range from 190 to 305 K, but is weakest over the great stratocumulus fields of the subtropical oceans, and has secondary maxima in the midlatitude storm tracks.

Figure 2c shows the amplitude of the annual mean diurnal cycle of the 11-μm brightness temperature. Diurnal variability dominates the total variance in desert locations, where surface temperature variations dominate the brightness temperature signal, and in tropical land regions, where diurnal convection results in cold brightness temperatures in the afternoon, when convection maximizes. In other regions, where synoptic-scale cloudiness variation dominates the signal, most variation is on longer time scales. This is illustrated in Fig. 3, which shows the large amplitude of diurnal variability in desert regions, and much smaller amplitude in tropical oceanic and midlatitude regions. The halo-like regions of high diurnal variability, especially noticeable at 60°N and Slatitude and at 60°E longitude, are artifacts of the satellite data merge processes and are discussed briefly below.

The annual mean amplitude of the semidiurnal cycle is shown in Fig. 2d. This amplitude is highly correlated with that of the diurnal variability, due to the asymmetric nature of the solar forcing of diurnal variability. Although the diurnal and semidiurnal components of brightness temperature variations are small relative to the total variance, they can introduce large errors into observations of annual mean brightness temperature. Figure 4 shows the errors in the annual mean brightness temperature that result if the GCI data are sampled twice daily. Figure 4a shows results for twice daily sampling at fixed times (local noon and midnight). Note the similarity of the pattern of error magnitude to the pattern of the semidiurnal cycle amplitude. In Fig. 4b, the sampling times advance through the day at a rate of 24 h yr^{-1}, while in Fig. 4c, they advance at a rate of 72 h yr^{-1}. Clearly, twice-daily sampling at fixed local time produces a far worse estimate of the annual mean than does sampling at varying times of day, but the speed of precession is of little consequence. This demonstrates that there is little annual variation in the phase of the diurnal brightness temperature cycle, since any such variations would combine with variation in the time of day of observations to give substantially larger errors for a single diurnal precession per year than for several precessions per year.

The large, spurious diurnal and semidiurnal variability in the regions at the edges of the range of geostationary satellites is due to details of the data processing algorithm's substitution of polar for geostationary satellite data (M. Salby 2001, personal communication). Because this large spurious semidiurnal variation will increase sampling errors, especially for sun-synchronous orbits, the use of the GCI data as a proxy for real brightness temperature variability results in an overestimate of the mean. However, the equally large errors over continental regions derive from real variability, so the conclusions we draw about which orbits best reduce sampling error are not affected by the spurious contributions.

Figure 5 shows that some observation times are bet-

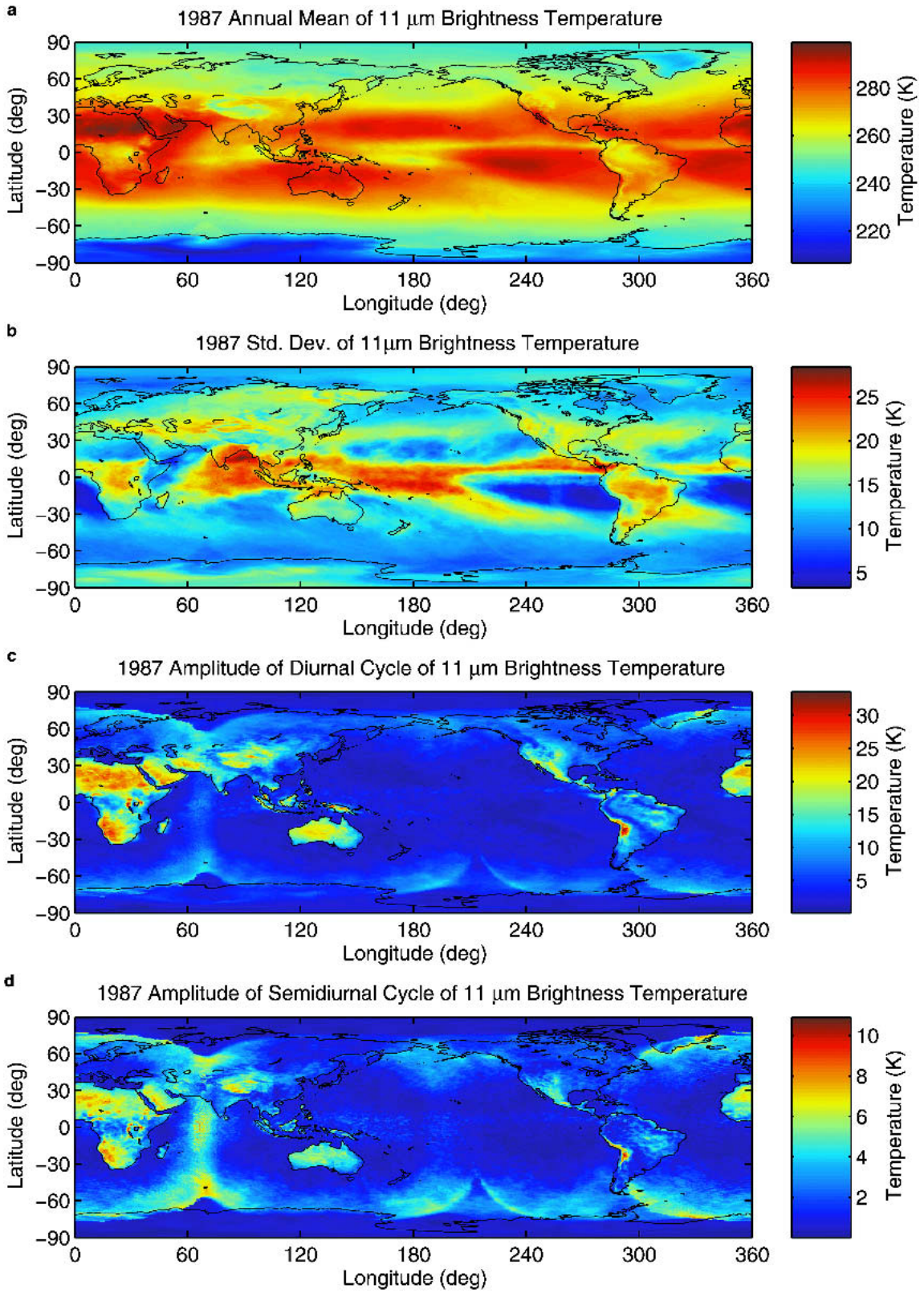

FIG. 2. (a) 1992 annual mean of global cloud imagery 11-μm brightness temperature, (b) standard deviation of brightness temperature, (c) amplitude of diurnal cycle, and (d) amplitude of semidiurnal cycle.

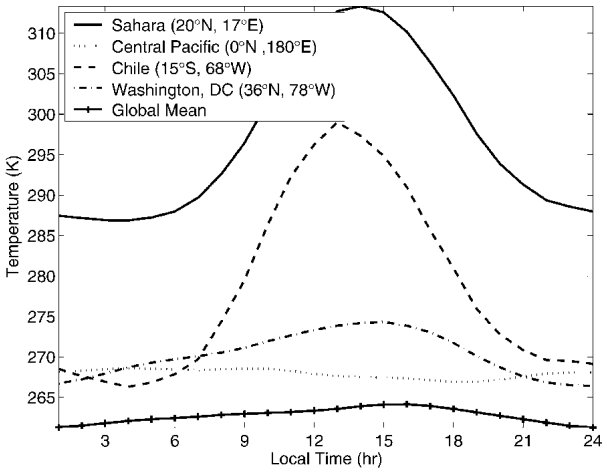

FIG. 3. Annual mean brightness temperature as a function of local time (interpolated from GCI data at 0000, 0300, 0600, 0900, 1200, 1500, 1800, 2100 UTC) for several locations (indicated in legend).

ter than others. It shows the observation time dependence of the standard deviation of the errors shown for noon and midnight observations in Fig. 4a. Clearly, a single sun-synchronous satellite making fixed time-of-day observations will more closely approximate the true average brightness temperature if its equator crossing times are set to 4 A.M./P.M. or 10 A.M./P.M., rather than 1 A.M./P.M. or 7 A.M./P.M. These times correspond to the nodes of the semidiurnal cycle in brightness temperature averaged over those regions where the diurnal cycle is of substantial amplitude (greater than 3 K).

4. Results and discussion

Our results are summarized in Figs. 6–9 and Tables 1–3. They present the statistical properties of the sampling errors modeled for a range of orbital parameters and for different sampling periods. We are looking for those orbital configurations that can recover brightness temperature with the fewest grid-point errors larger than 0.1 K. We are interested both in the absolute accuracy, and in the accuracy of difference from one year to the next. The grid resolution is 15° latitude by 30° longitude. Table 1 defines the alphabetical labels for the various orbit and scanning combinations. Tables 2 and 3 show the standard deviation over all grid squares, of sampling errors for mean, diurnal minimum, and diurnal range of brightness temperature. Figures 6–9 show the distribution of these grid-square errors. In the figures, the errors are shown for three different years (1987, 1988, and 1992), or three year-to-year differences (1988–87, 1992–87, 1992–88), while in the Tables 2 and 3, the mean of standard deviations for the three years—or three differences—is shown. For both the tables and figures, various averaging periods, orbits, numbers of satellites, and sampling patterns (nadir or cross-track scanning) are shown. In Figs. 6–9, for each distribution, the central dot corresponds to the median of the grid-square errors, and the lines extend from the minimum to the 25th percentile and from the 75th percentile to the maximum error.

a. Errors of annual means

Figures 10 and 11 show annual mean errors for a single satellite in various orbits. Figures 10 and 11a show the impact of spatial averaging on errors. In each figure, errors for a single sun-synchronous satellite with 2 A.M./P.M. equator-crossing times are shown. In Fig. 10, the standard deviation of the errors is 3.8 K. Much of this error is due to random variations in the brightness temperature, thus, errors in adjacent grid squares are uncorrelated. If the satellite observations are averaged over larger spatial regions, the errors decrease substantially. Figure 11a shows errors of 15° latitude by 30° longitude grid squares. The standard deviation of these errors is reduced to 0.5 K. All further results will refer to brightness temperature averaged over grid squares of this size unless otherwise noted. We will frequently compare errors to a standard of 0.1 K, since this accuracy could potentially allow discrimination of regional trends differing by, for example, 0.5 K decade^{-1} within 2 yr, and global trends differing by 1 K century^{-1} within 10 yr.

We first consider errors in annual mean brightness temperature for a single satellite in various orbits, shown in Fig. 11. As predicted by Fig. 5, which compared idealized results for different local time observations, a single sun-synchronous satellite with 4 A.M./P.M. equator crossing times (Fig. 11a) does substantially better than one with 6 A.M./P.M. equator crossing times (Fig. 11b). As predicted by Fig. 4, which compares results for twice-daily sampling at fixed and precessing local times, a single precessing polar orbiter (Fig. 11c) is clearly superior to either sun-synchronous orbiter. Comparison of these figures clearly shows the distinction between random errors and errors due to aliasing of diurnal variability. If the resolution of the errors due to twice-daily sampling shown in Figs. 4 and 5 is degraded to 15° by 30°, we find the following. Twice or thrice yearly precessing sampling times result in errors whose standard deviation is less than 0.1 K, while a polar orbiter, whose observation times precess twice yearly gets errors at this resolution of over 0.2 K: this difference is due to the single orbiter's inadequate total observation density. On the other hand, the errors for fixed local time observation explain 80% of the variance in Fig. 11a, showing the role of diurnal sampling bias.

A low-latitude precessing orbiter (Fig. 11d) does not produce substantially better annual mean brightness temperatures than a polar orbiter, even in the region where its observations are concentrated. This is because a single full precession of the time of observation

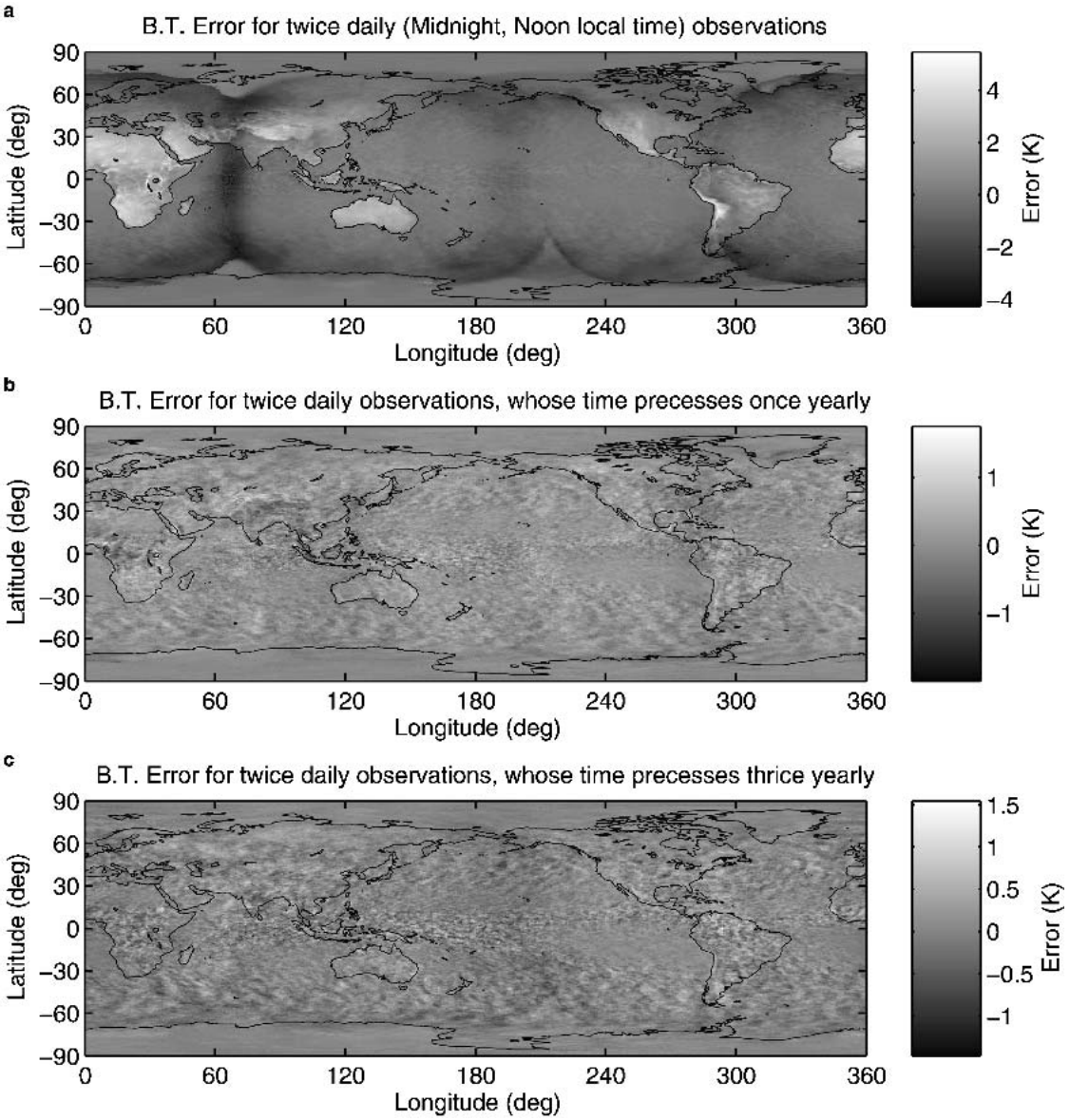

FIG. 4. Error in annual mean brightness temperature for twice-daily sampling, with histograms of error to right. (a) No precession, sampling at local noon and midnight; (b) twice-daily sampling, phase shifts over one diurnal cycle over the year; and (c) twice-daily sampling, phase shifts over three diurnal cycles over the year.

over the course of a year is sufficient to eliminate most of the sampling bias, and further precessions do little to reduce the error. Further confirmation of this comes from considering the error for an 81° orbit. For this orbit, the reverse of a sun-synchronous orbit (the orbit's angle of inclination is the same, but the satellite orbits in the opposite sense), the orbital plane precesses twice in a year. Table 2 and Fig. 6 show that this orbit (labeled **D**) gives slightly larger errors than a 90° polar orbiter (labeled **C**). These larger errors are due to the reduced coverage in polar regions, where a 90° polar orbiter has very small errors. None of the orbits shown in Fig. 11 allows a single orbiter to achieve 0.1 K accuracy in brightness temperature at all locations. We next inquire whether regions with small errors in one year tend to have small errors in other years. Figure 12 shows that the bias errors for a sun-synchronous orbit are substantially reduced for trend observations. Errors for the year 1992 are plotted point-by-point against errors for the year 1987. The polar orbiting model satellite errors are uncorrelated, so that one cannot expect a region with low errors in one year to have low errors in another. While the sun-synchronous satellite produces highly correlated errors, the errors remaining after the linear relationship between the two years' errors is removed are still slightly larger than those of the polar

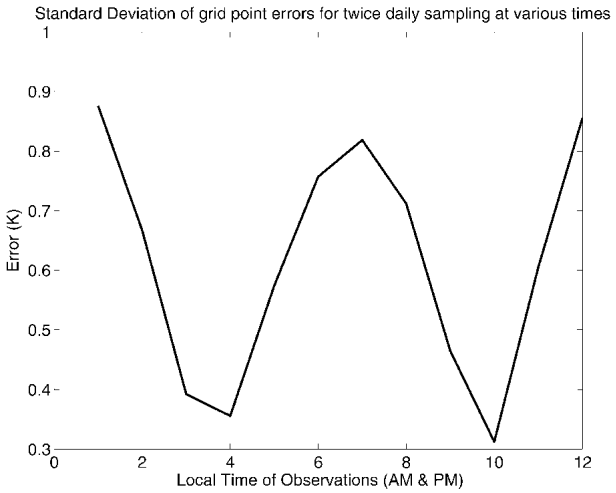

FIG. 5. Standard deviation of grid point errors (at 0.35° lat by 0.7° lon resolution) of twice-daily sampling (as in Fig. 3a) plotted as a function of time of day of the equator crossings.

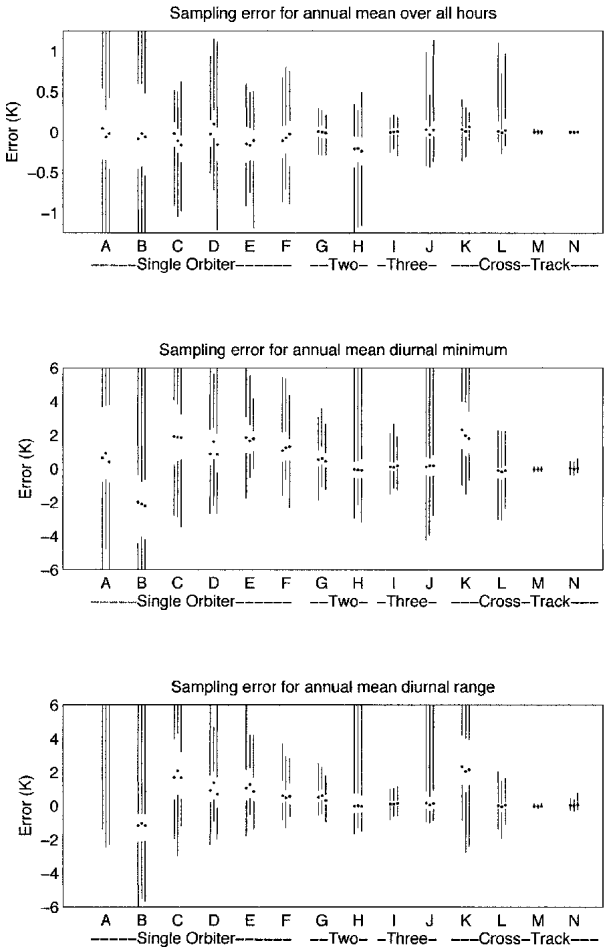

FIG. 6. The distribution of errors in mean brightness temperature, average daily minimum brightness temperature, and average diurnal brightness temperature range are plotted for a number of satellite orbits and for three different years. Errors are in kelvin, and are for averages over grid squares spanning 15° lat and 30° lon. For each year and orbit, the lower line spans the range from the minimum (largest negative) error over all grid squares to the 25th percentile, the point shows the median error, and the upper line spans the range from the 74th percentile to the maximum error. The years plotted are, from left to right, 1987, 1988, and 1992. The orbit combinations are labeled on the x axis by capital letters, which correspond to obits shown in Table 1.

orbiter (0.4 versus 0.3 K), due to interannual variability in the diurnal cycle.

As discussed by Leroy (2001) and by Vinnikov and Grody (2003), accuracy in interannual trends for sun-synchronous satellites is dependent on the restriction of orbit drift to small values. Figure 13 shows that while annual means derived from precessing satellites are insensitive to orbital drift, drift in sun-synchronous satellites causes errors in year-to-year differences of about 0.2 K h^{-1} of drift in equator-crossing time. For 3-month means, a 90° polar orbiter has not yet fully sampled the diurnal cycle, so errors due to drift are only slightly smaller than for a sun-synchronous satellite.

To obtain greater accuracy in retrieved brightness temperature, we consider the sampling errors for observations by multiple satellites. Figure 14 shows results for two polar satellites, orbiting at 90° angles in longitude, for three polar satellites orbiting at 60° angles, and for three sun-synchronous satellites orbiting at 60° angles. Two polar orbiters produce errors that are always less than 0.35 K, with 65% of errors less than 0.1 K. The angular separation is important for the reduction of diurnal sampling bias: two sun-synchronous orbiters separated by 6 h in equator-crossing time produce errors with a standard deviation of 0.2 K, while two orbiters with equator crossing times of 10:30 and 1:30 (the NASA Terra and Aqua orbits, respectively) produce errors of 0.7 K. Three 90° polar orbiters produce errors than are always less than 0.21 K, with 84% or errors less than 0.1 K. However, for three sun-synchronous orbiters, the maximum error is 0.87 K, and only 30% of errors are less than 0.1 K. Another way to reduce errors is to average over still larger spatial regions. Retrieval errors for zonal averages are given in Fig. 15. Zonal mean errors are universally less than 0.1 K for two or for three polar satellites, and also for a single low-latitude orbiter. A single polar satellite, or three sun-synchronous satellites, can attain zonal mean brightness temperature averages with less than 0.2-K sampling error. We have also simulated the sampling errors of cross-track scanning satellites. For sun-synchronous orbits, these perform only marginally better than nadir-sampling satellites: for annual mean retrieval, and a 20° wide cross-track scan, Table 2 shows that the standard deviation of errors at 30° × 15° resolution is 0.20 K for three cross-track scanning satellites, and 0.21 K for three nadir-viewing satellites. As discussed by Leroy (2001), cross-track scanning of practical width does not extend the range of the time of day

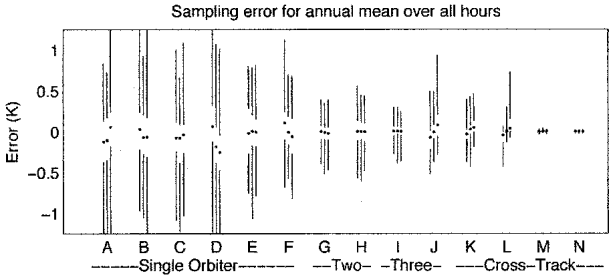

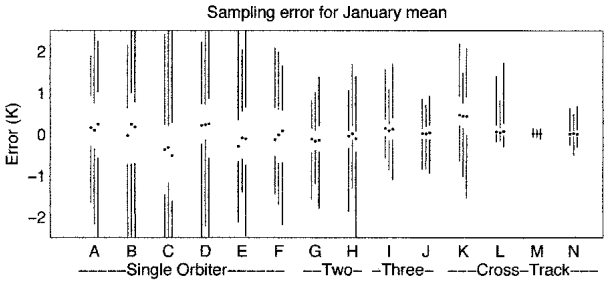

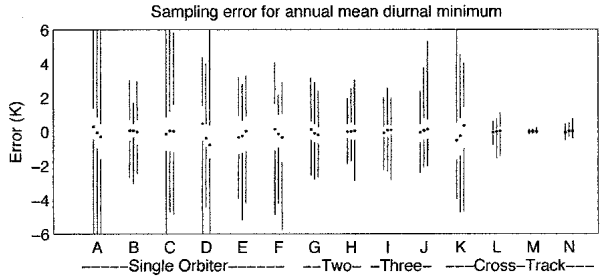

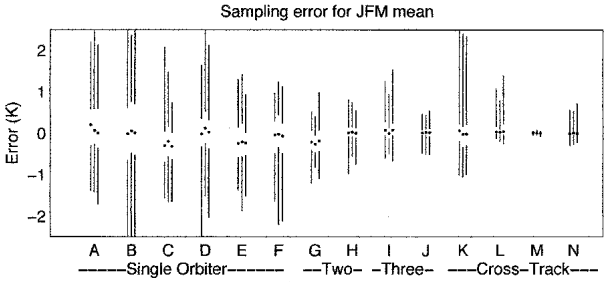

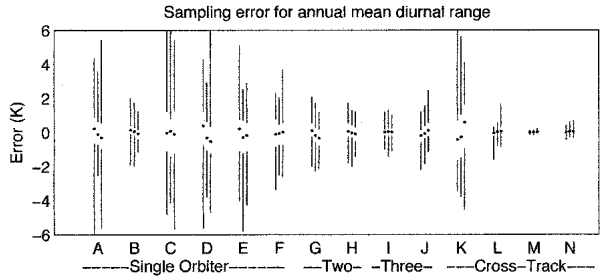

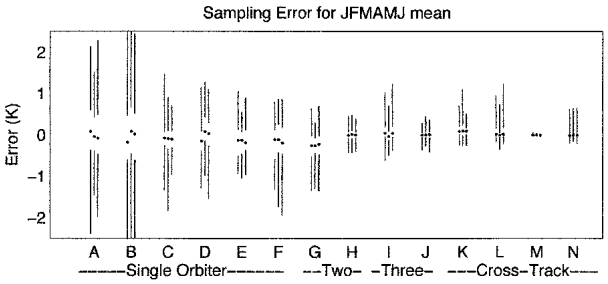

FIG. 7. As in Fig. 5 but year differences rather than annual means are plotted. From left to right, the differences are 1988–87, 1992–88, and 1992–87.

FIG. 8. As in Fig. 5 but errors are for grid square mean errors for the month of Jan, the months Jan–Mar, and the months Jan–Jun.

of observation sufficiently to reduce the systematic biases that cause large errors for sun-synchronous orbits. For precessing orbits, systematic sampling bias has been largely removed, so cross-track scanning can substantially reduce errors by increasing the number of observations, thus reducing error due to weather noise (nonperiodic real variations in brightness temperature). Thus even a single cross-track scanning satellite in a 90° polar orbit (**K**) can produce brightness temperature errors whose standard deviation is less than 0.1 K. However, the calculated errors account for sampling only, and do not take into account bias due to the angle of view, as we discuss briefly below.

b. Errors of monthly, seasonal, and semi-annual means

Results for shorter averaging periods show some distinct differences from those for annual means. Of course, since the number of observations is smaller, mean errors, shown in Table 3 and Figs. 8 and 9 for a range of orbital configurations and averaging periods, are correspondingly larger so that at least three satellites are required to achieve high accuracy. Three further results stand out. First, retrievals from polar orbiting satellites improve much more rapidly with increased averaging time than do retrievals from sun-synchronous satellites, consistent with the strong diurnal sampling bias of sun-synchronous satellites discussed in the previous section—a polar orbiter does not precess far enough in a single month to reduce diurnal sampling bias, but after 6 months a complete precession has been accomplished, and diurnal sampling bias is substantially reduced. Second, sun-synchronous satellites do substantially better at retrieving differences between years than at retrieving absolute brightness temperature, though still not so well as polar orbiting satellites. For a 1-month average, retrievals from a single tropical orbiter produces errors much smaller than for a single polar orbiter, and errors comparable to those from two polar orbiters. This follows from the relatively rapid

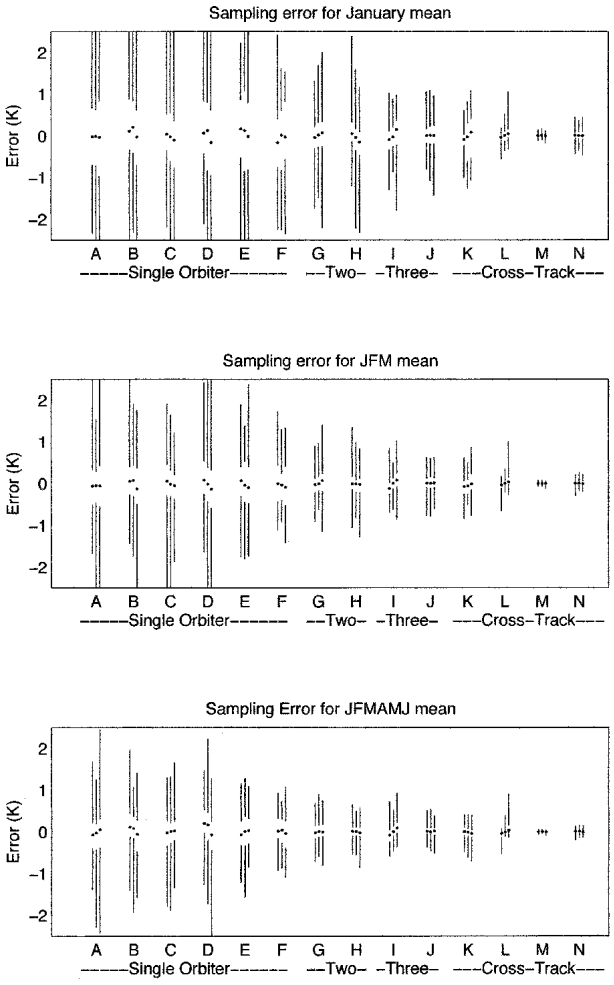

FIG. 9. As in Fig. 7 but year differences rather than single year means are plotted. From left to right, the differences are 1998–87, 1992–88, and 1992–87.

precession of a tropical orbiter, which allows adequate sampling of the diurnal cycle by a single orbiter in a 3-month period, and the higher frequency of observations achievable by covering a smaller fraction of the earth's surface area.

c. *Errors of mean diurnal variability*

Obtaining high accuracy for means sorted by time of day is more difficult than for means over all times of day. The number of observations available at a given time of day is reduced by an order of magnitude from the total number of observations, which increases sampling errors due to random variability. In addition, the binning of observations at a range of local times into a finite number of time-resolved means can add systematic errors. Table 2 and Figs. 8 and 9 show that precessing orbits are superior to sun-synchronous orbits for constructing climate means of diurnal variability, but

TABLE 1. Satellite orbit labels for Tufte plots of error distributions for various orbits and years (Figs. 9–12).

Label	Orbit description
A	One sun-synchronous, 4 A.M./P.M. equator crossing time
B	One sun-synchronous, 6 A.M./P.M. equator crossing time
C	One 90° precessing polar orbiter
D	One 81° precessing polar orbiter
E	One 53° precessing orbiter
F	One 33° precessing tropical orbiter
G	Two sun-synchronous polar orbiters (6 and 12 A.M./P.M. equator crossing times.
H	Two 90° precessing polar orbiters, with 90° lon separation.
I	Three sun-synchronous polar orbiters (6, 10, 2 A.M./P.M. equator crossing times)
J	Three 90° precessing polar orbiters, with 120° lon separation.
K	One cross-track-scanning 90° precessing polar orbiter
L	Three cross-track-scanning sun-synchronous polar orbiters
M	Three cross-track-scanning 90° precessing polar orbiters
N	Ten equally spaced nadir-viewing sun-synchronous orbiters

that nadir-viewing alone cannot produce high accuracy time-of-day resolved observations of infrared radiance for a small number of satellites. For this application, both a large number of observations and observations distributed at all local time throughout the year are needed. Thus, while a single precessing cross track scanning satellite can recover the annual mean brightness temperature with typical errors of ~0.1 K, its errors in recovering the annual mean diurnal temperature range are typically ~3 K, much larger than for three nadir-viewing precessing orbiters, despite 8 times more observations. Three cross-track scanners do a far better job, achieving 0.5-K accuracy in the diurnal range for sun-synchronous orbiters and 0.1-K accuracy for precessing 90° polar orbiters.

Interannual differences in these quantities can be measured accurately by sun-synchronous satellites, assuming equator-crossing times are held constant. Our calculations have not addressed the systematic error introduced by the variation of viewing angle for cross-track scanning radiometers. Some correction of the resulting biases should be possible using 24-h annual mean values, since for this statistic observations taken at a fixed viewing angle from three satellites would be sufficient to reduce sampling errors over all times of day to ~0.1 K, and so the viewing angle bias could be found to this accuracy. The correction will be more difficult for the diurnally varying component of the viewing angle bias, since observations at nadir only are not sufficient in this case to reduce errors to small values unless approximately 10 satellites are flown.

5. Conclusions

A major goal of climate science for the coming decade is to reduce the uncertainty concerning the sensi-

TABLE 2. Standard deviation of 30° × 15° grid box errors for annual mean, annual mean minimum, and annual mean diurnal range of brightness temperature (BT) and for year-to-year differences.

	Errors of					
Orbit	Annual mean BT	Differences of annual mean BT	Annual mean minimum BT	Differences of annual mean minimum BT	Annual mean diurnal BT range	Differences of annual mean diurnal BT range
A	0.56	0.42	4.18	1.87	—	1.28
B	1.01	0.40	2.51	0.78	—	0.48
C	0.26	0.33	1.51	1.21	2.85	1.81
D	0.30	0.43	1.05	1.19	1.40	1.48
E	0.32	0.34	0.79	1.00	1.28	1.52
F	0.25	0.35	0.72	1.00	1.11	1.53
G	0.26	0.17	1.89	0.91	—	0.96
H	0.11	0.15	0.45	0.55	0.52	0.65
I	0.20	0.16	1.06	0.52	—	0.59
J	0.07	0.10	0.31	0.38	0.29	0.37
K	0.09	0.11	1.31	1.02	2.61	1.84
L	0.21	0.11	0.68	0.30	0.53	0.28
M	0.01	0.01	0.08	0.10	0.11	0.15
N	0.04	0.03	0.12	0.15	0.14	0.17

TABLE 3. Standard deviation of 30° × 15° grid box errors in BT for various orbits; for averaging periods of 1, 3, and 6 months; and for differences from year to year.

	Error of					
Orbit	Jan mean BT	Differences of Jan mean BT	Jan–Mar mean BT	Differences of Jan–Mar mean BT	Jan–Jun mean BT	Differences of Jan–Jun mean BT
A	0.95	1.16	0.71	0.73	0.67	0.59
B	1.20	1.06	1.08	0.68	1.05	0.56
C	1.28	0.97	0.56	0.64	0.37	0.47
D	1.06	1.39	0.62	0.85	0.45	0.61
E	0.95	1.28	0.55	0.69	0.39	0.49
F	0.80	1.01	0.46	0.68	0.35	0.47
G	0.44	0.52	0.33	0.32	0.31	0.25
H	0.45	0.53	0.22	0.31	0.14	0.20
I	0.36	0.39	0.27	0.25	0.23	0.20
J	0.28	0.38	0.15	0.22	0.11	0.16
K	0.58	0.44	0.54	0.25	0.17	0.15
L	0.25	0.17	0.22	0.13	0.22	0.12
M	0.04	0.05	0.02	0.03	0.02	0.02
N	0.13	0.13	0.13	0.07	0.13	0.05

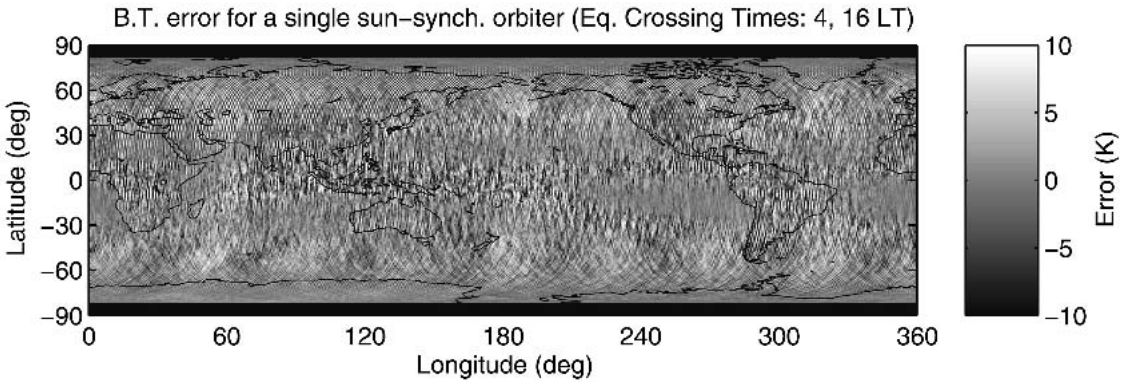

FIG. 10. Retrieval errors for annual mean 11-μm brightness temperature for a single sun-synchronous satellite.

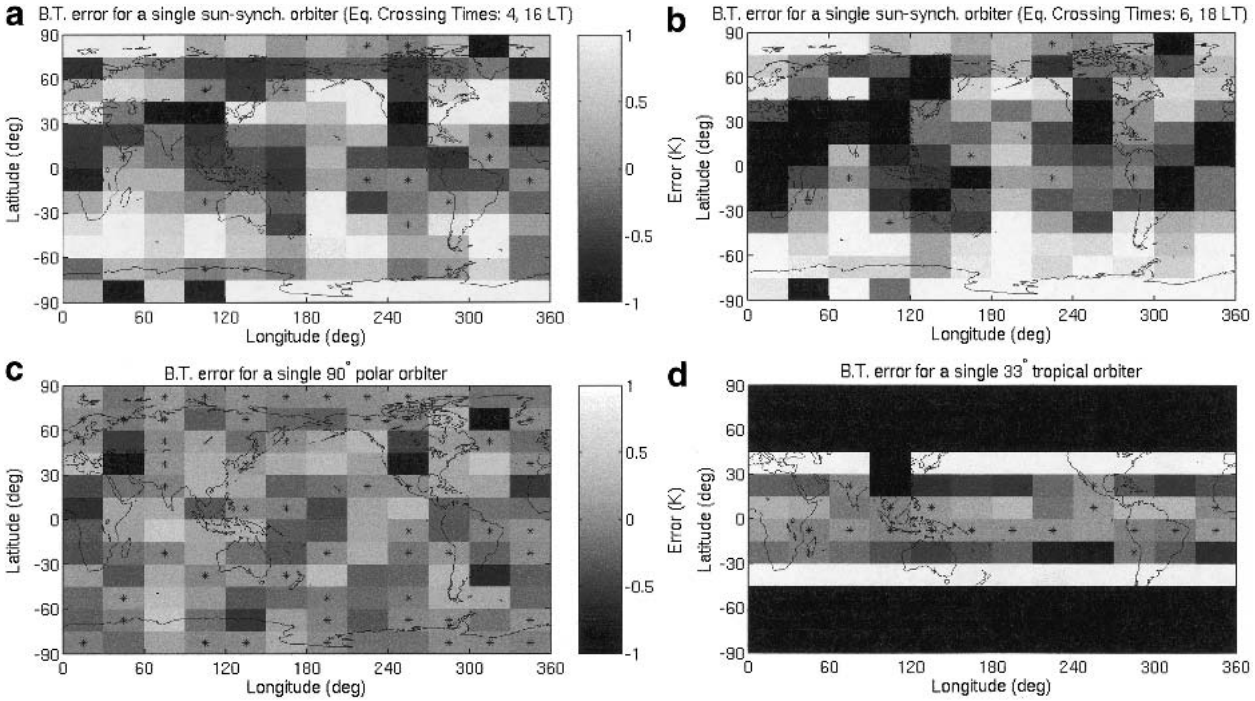

FIG. 11. Retrieval errors for 1992 annual mean 11-μm brightness temperature for a single satellite. The grid boxes are 15° lat by 30° lon. A sampling error less than 0.1 K is distinguished with an asterisk (*): (a) a single sun-synchronous orbiter (inclination: 98.765°, altitude: 833 km), equator-crossing time 4 A.M./P.M.; (b) same as (a) but equator crossing time 6 A.M./P.M.; (c) a single polar orbiter (inclination: 90°, altitude: 833 km); and (d) a single tropical orbiter (inclination: 33°, altitude 662 km).

tivity of the earth's climate to increasing greenhouse gas concentrations. To accomplish this will require highly accurate observations of the actual state of the earth's climate. Observations of spectrally resolved infrared radiance may make a vital contribution to this requirement (Anderson et al. 2004). We have shown that reasonable number of satellites can achieve sampling accuracy of 0.1 K with adequate spatial resolution. This should focus renewed attention on the fundamental accuracy of radiance measurements from space, so that end-to-end accuracy can be made to achieve this threshold.

Both random errors due to weather noise and bias are present in our sampling of the GCI dataset. Random errors can be reduced only by increasing the

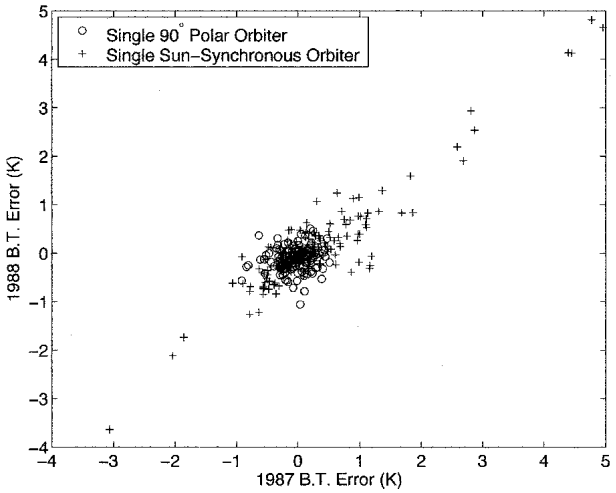

FIG. 12. Scatterplot of errors for 1987 data vs errors for 1988 data. Errors for a single sun-synchronous satellite are shown with open circles, while errors for a single polar orbiting satellite are shown with plus signs.

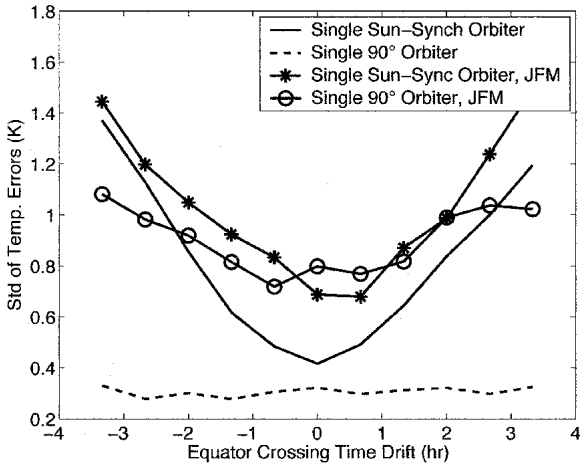

FIG. 13. Variation with orbital drift of the standard deviation of the errors for difference of 1988 and 1987 annual mean (solid and dashed lines) and Jan–Mar mean (solid lines with circles and asterisks) brightness temperature in 15° lat by 30° lon grid boxes.

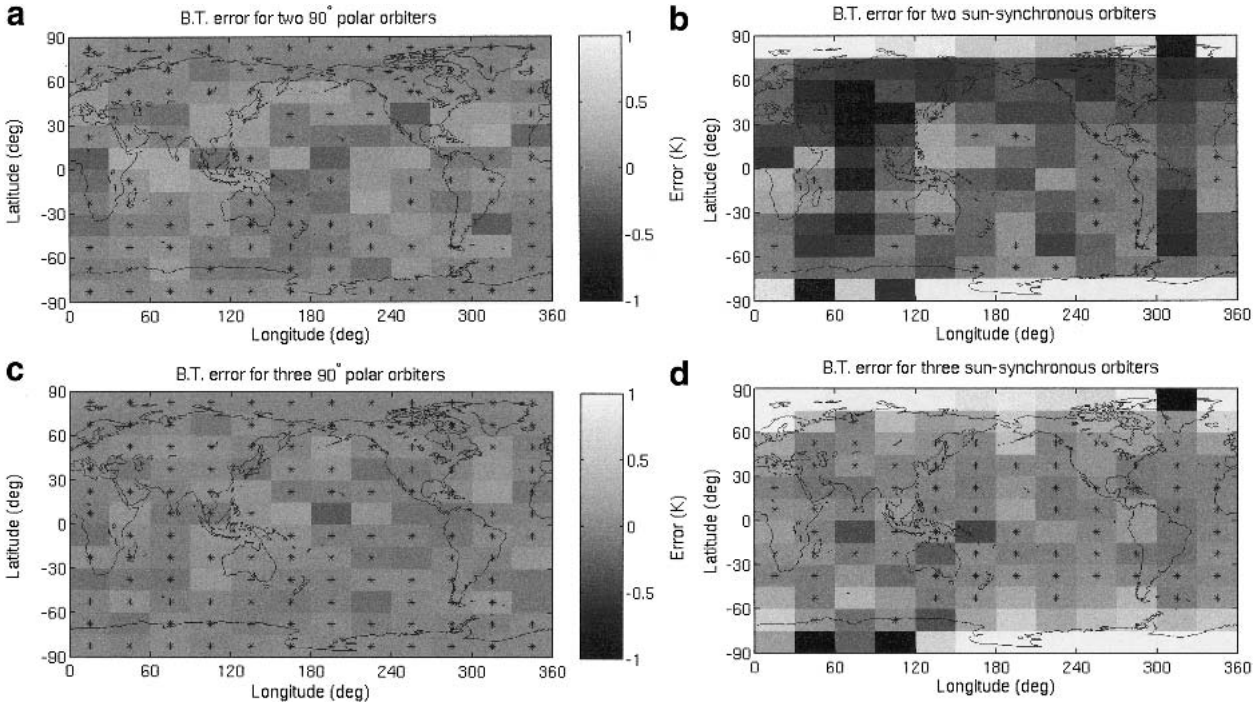

FIG. 14. As in Fig. 9 but for suites of satellites equally spaced in longitude: (a) two sun-synchronous polar orbiters (inclination 98.765°, altitude 833 km), (b) two polar orbiters (altitude 833 km), (c) three polar orbiters, and (d) three sun-synchronous polar orbiters.

number of observations, while bias can be reduced by careful selection of observation patterns. We have shown that the primary source of sampling bias in the construction of monthly to annual means over all times of day is the aliasing of the semidiurnal variability onto the mean due to inadequate sampling of the diurnal cycle. Thus, when observations are scattered through all times of day, as they are for a 90° polar orbiter, the systematic errors are greatly reduced. Reduction of random errors due to weather noise below 0.1 at 30° × 15° spatial resolution requires three satellites.

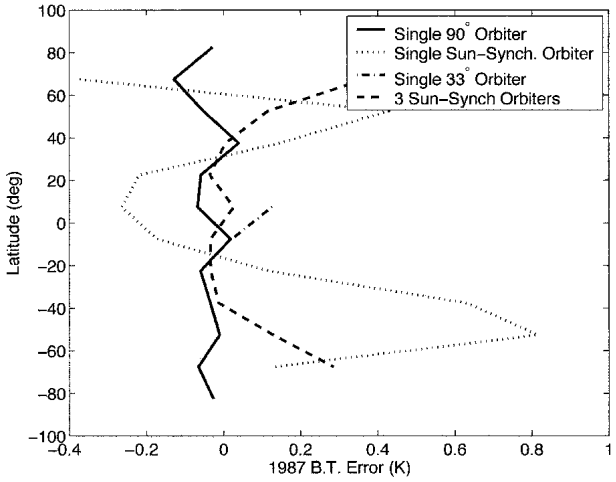

FIG. 15. Zonal mean annual-mean sampling errors for 11-μm radiance temperature for 1992 for various satellite orbits, as labeled in legend.

We conclude from the results presented above that the sparse sampling of brightness temperature from a small number of orbiting radiometers places an important constraint on the accuracy of benchmark radiance measurements. If only a single orbiter is to be flown, the precessing polar orbit represents the best choice to minimize sampling errors and their zonal means. Substantial increases in the spatial resolution at which 0.1-K accuracy can be obtained are achieved by adding orbiters. To be confident of this level of accuracy at nearly all geographic locations requires a constellation of three precessing polar orbiters.

Satellites designed for weather prediction are generally placed in sun-synchronous orbits because of the need to emphasize changes occurring on time scales of a few days. However, the canonical meteorological constellation of three sun-synchronous satellites clearly compromises climate investigations. Averages for individual climate regions can show large errors, which are only partially reproducible from year to year. However, if repeatable errors can be eliminated (using spectrally resolved data taken from geostationary orbit), or if zonal means can be taken, annual mean sampling errors of less than 0.2 K are feasible for three sun-synchronous satellites. Error corrections along the lines of Mears et al. (2003) and Vinnikov and Grody (2003) may further reduce these errors, though such corrections are vulnerable to model deficiencies.

These limitations apply to radiances that originate at the surface or at clouds and which have large diurnal variations. Radiances that are not affected by clouds or the surface (e.g., MSU radiances, or GPS radio occultation) may show smaller errors. For these, sun-synchronous satellites may provide acceptable climate data.

Acknowledgments. The authors are grateful to Murry Salby for the use of his Global Cloud Imagery dataset.

Support has been provided by NASA Grant NAG5-8779, and NOAA Contract 50-SPNA-1-00042. Helpful reviews by Stephen Leroy and an anonymous reviewer improved the clarity and completeness of this paper.

REFERENCES

Anderson, J. G., J. Dykema, R. M. Goody, H. Hu, and D. B. Kirk-Davidoff, 2004: Absolute, spectrally resolved, thermal radiance: A benchmark for climate monitoring from space. *J. Quant. Spectrosc. Radiat. Transfer,* **85,** 367–383.

Chang, T. C., L. S. Chiu, C. Kummerow, J. Meng, and T. T. Wilheit, 1998: First results of the TRMM Microwave Imager (TMI) monthly oceanic rain rate: comparison with SSM/I. *Geophys. Res. Lett.,* **26,** 2379–2382.

Christy, J. R., R. W. Spencer, W. B. Norris, W. D. Braswell, and D. E. Parker, 2003: Error estimates of version 5.0 of MSU-AMSU bulk atmospheric temperatures. *J. Atmos. Oceanic Technol.,* **20,** 613–629.

Hanel, R. A., B. J. Conrath, V. G. Kunde, C. Prabhakara, I. Revah, V. V. Salomonson, and G. Wolford, 1972: The Nimbus 4 infrared spectroscopy experiment, Part I: Calibrated thermal emission spectra. *J. Geophys. Res.,* **77,** 2629–2641.

Haskins, R., R. M. Goody, and L. Chen, 1999: Radiance covariance and climate models. *J. Climate,* **12,** 1409–1422.

Heiskanen, W. A., and H. Moritz, 1967: *Physical Geodesy.* W.H. Freeman and Company, 364 pp.

Leroy, S. S., 2001: The effects of orbital precession on remote climate monitoring. *J. Climate,* **40,** 4330–4337.

Mears, C. A., M. C. Schabel, and F. J. Wentz, 2003: Analysis of the MSU channel 2 tropospheric temperature record. *J. Climate,* **16,** 3650–3664.

Salby, M. L., H. H. Hendon, K. Woodberry, and K. Tanaka, 1991: Analysis of global cloud imagery from multiple satellites. *Bull. Amer. Meteor. Soc.,* **72,** 467–480.

——, and P. Callaghan, 1997: Sampling error in climate properties derived from satellite measurements: Consequences of under sampled diurnal variability. *J. Climate,* **10,** 18–35.

Vinnikov, K. Y., and N. C. Grody, 2003: Global warming trend of mean tropospheric temperature observed by satellites. *Science,* **302,** 269–272.

——, A. Robock, N. C. Grody, and A. Basist, 2004: Analysis of diurnal and seasonal cycles and trends in climatic records with arbitrary observation times. *J. Geophys. Res.,* **31,** L06205, doi:10.1029/2003GL019196.